



Heat transfer characteristics for double water-jets on thick plates with various jet velocities and heights

Xiuhua Tian¹ · Tianliang Fu¹ · Zhaodong Wang¹ · Guodong Wang¹

Received: 16 September 2020 / Accepted: 20 March 2021 / Published online: 9 April 2021
© The Author(s), under exclusive licence to Springer-Verlag GmbH Germany, part of Springer Nature 2021

Abstract

During cooling, the array jet impact can achieve a rapid and uniform cooling of the high-temperature plate. Previous research results mostly focused on single-jet cooling of thin plates, but the complex flow and heat transfer characteristics between multiple jets could not be obtained. To clarify the heat transfer mechanisms and cooling speed fields characteristics in different flow regions, double water-jet impingement experiments were carried out on an AISI 304 austenitic stainless-steel plate with a thickness of 50 mm. The jet exit velocity was set to 2.95, 5.90, 8.06, and 11.80 m/s, while the jet height was set to 50, 150, 250, 350, and 450 mm. Pure water was selected as the working fluid with a constant temperature of 12.8 °C. The results show that a complex trend with sequential increasing, decreasing, and increasing behaviors appears in the wetting front width, upon increasing the wetting region diameter. The confluence fluid was found to reduce the influence caused by different jet velocities and to increase the influence caused by different jet heights. In addition, it was found that an excessive amount of accumulated fluid reduces the heat transfer efficiency during transition boiling. Finally, the correlations between maximum heat flux and average maximum cooling speed were established, which provide useful data for optimizing the cooling technology.

Keywords Thick plate · Jet velocity · Jet height · Rewetting · Cooling speed peak

1 Introduction

Impinging jet cooling is a widely used technique in heat treatment processes owing to the wide range of controllability of the cooling speed. When a single circular jet impinges on a solid surface, the fluid spreads around the wall. The flow can be divided into stagnation region, acceleration region, and wall jet region. The stagnation point coincides with the jet point and exhibits the maximum pressure [1]. In the accelerating region, the flow velocity increases gradually along the radial direction until it approaches the jet velocity. In the wall jet region, the fluid flows along the radial direction with a decreased velocity caused by the viscous force.

When the low-temperature fluid contacts the high-temperature wall, a vapor film will form, which limits the heat

transfer between fluid and wall. After the collapse of the vapor film, the fluid can contact the hot surface again, which is known as a rewetting phenomenon [2]. More effective surface cooling occurs when the hot surface is rewetted. The cooling process is gradually carried out along the radial direction from the jet point. When the surface temperature downstream reaches the rewetting temperature, the rewetting will extend to the downstream [3]. Different cooling times result in different boiling structures on the surface at the same time, including nucleate boiling, transition boiling, and film boiling. The wetting front is located between the dry and wet regions [4], and the whole transition boiling region is located at a point that can be considered as being part of the wetting front [5]. In the dry region outside the wetting front, since the surface temperature is higher than the minimum temperature for film boiling, a continuous vapor film is formed, and the fluid flows over it. The wet region is inside the wetting front, where nucleate boiling occurs.

The peak of the heat flux curve during cooling is referred to as the maximum heat flux, which is often used to characterize the surface quenching ability [6]. It is traditionally believed that the maximum heat flux occurs at the boundary between

✉ Tianliang Fu
futianliang@126.com

¹ State Key Laboratory of Rolling and Automation, Northeastern University, 110819 Shenyang, China

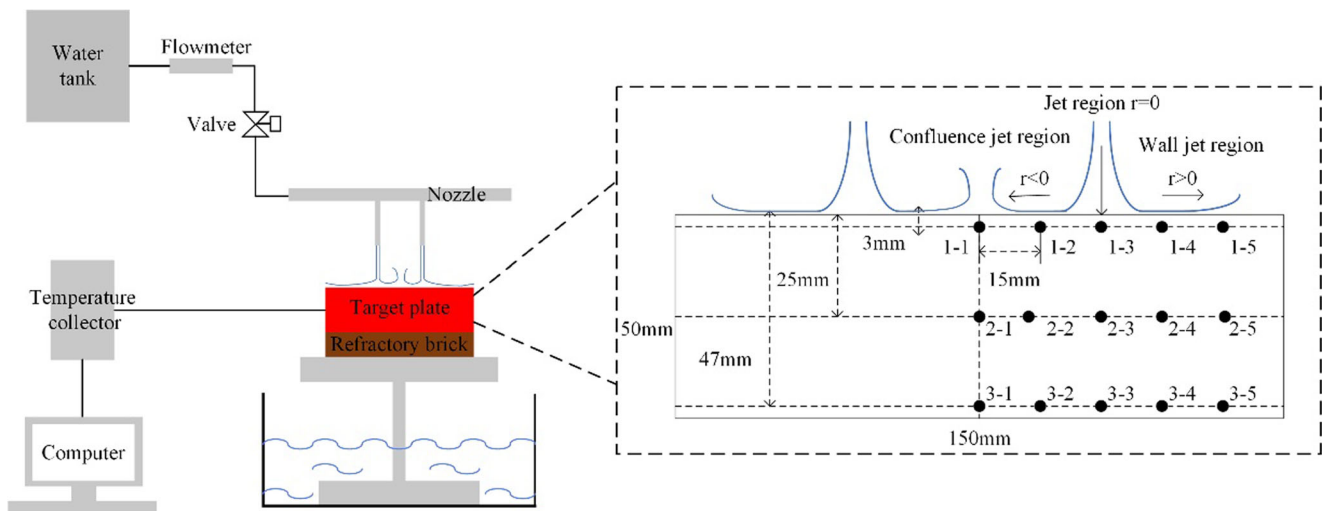


Fig. 1 Experimental layout

nucleate boiling and transition boiling. When the surface is in a nucleate boiling state, a higher heat transfer efficiency can occur under a relatively low wall-fluid temperature difference [7]. Therefore, one approach to improve the heat transfer efficiency is to increase the rewetting speed in order to induce the wall to enter the nucleate boiling state at an earlier time. At present, the movement mechanism of the wetting front is still not clear [8]. Woodfield et al. [9] reported that the increase of the radial temperature gradient causes a decreased wetting front width. Karwa et al. [10] found that the ability for the fluid to sweep bubbles at the wetting front might determine the moving speed of the wetting front. Hatta et al. [11] found that, when the wetting region is spread to 80 mm, the wetting front width increases to 20 mm, and they claimed that the decreasing flow velocity would lead to an increasing width. Several studies have analyzed the single-jet impingement heat transfer and found that the jet diameter, jet angle, jet velocity, and other parameters can affect the heat transfer ability [12–14]. In addition, several researchers have proposed correlations of the maximum heat flux for different experimental conditions. Agrawal et al. [15] and Paul et al. [16] found correlations between the jet height and heat flux. According to the flow velocity, supercooling, and superheat, Wang et al. [17] proposed a correlation to predict the surface heat flux.

In this study, double water-jet cooling experiments were performed using jet exit velocities of 2.95, 5.90, 8.06, and 11.80 m/s and jet heights of 50, 150, 250, 350, and 450 mm

on a 50 mm thick AISI 304 austenitic stainless-steel plate. The stagnation and acceleration regions are here denoted as the jet region, the region where the two jets interact is referred to as the confluence jet region, and the outside flow region without interference is denoted as the wall jet region. The rewetting phenomenon and heat exchange process for the different flow regions were discussed, and the results provide data and basis for optimizing the cooling technology of thick plates.

2 Experimental materials and methods

The chosen stainless steel was of grade 304, with specifications of 50 (thickness) \times 80 (width) \times 150 (length) mm³. The density ρ_s of the experimental material was 7930 kg·m⁻³. The specific heat c_s and thermal conductivity λ_s were calculated according to Eqs. (1) and (2) [18]. Temperature-measured holes with a diameter of 3.2 mm and depth of 40 mm were drilled at $h = 3, 25,$ and 47 mm to install thermocouples, as shown in Fig. 1. h is the distance to the cooled surface, while r represents the horizontal distance between the surface position and jet point. Symbols “-” and “+” indicate that the position is located in the confluence jet region or wall jet region, respectively. The embedded thermocouples were inserted into the holes parallel to the surface, and the gap was filled with high-temperature glue to further secure the thermocouples. Pure water with a constant temperature of 12.8 °C was selected as the working fluid.

Table 1 Experimental parameters

Variable	Test 1	Test 2	Test 3	Test 4	Test 5	Test 6	Test 7	Test 8
Q (L/h)	75	150	205	300	205	205	205	205
u (m/s)	2.95	5.90	8.06	11.80	8.06	8.06	8.06	8.06
z (mm)	150	150	150	150	50	250	350	450

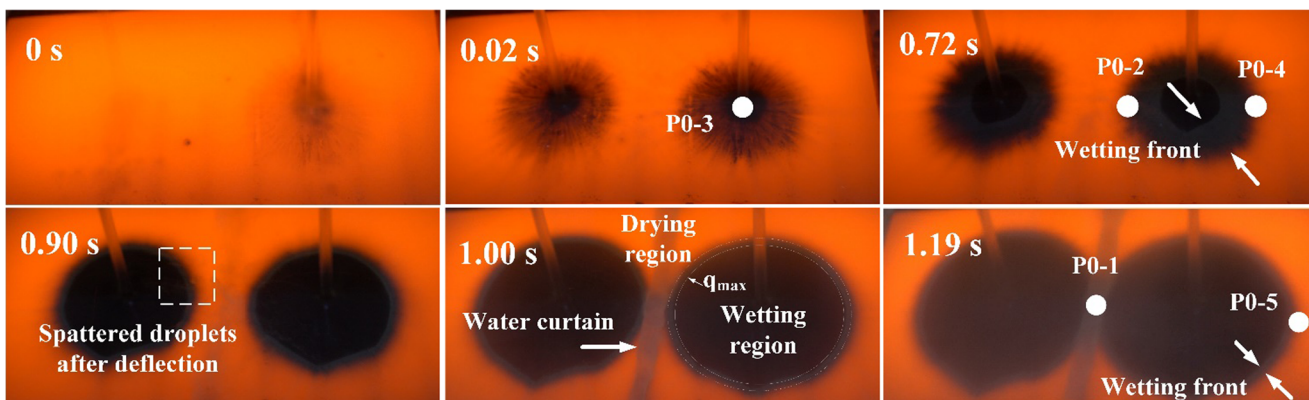


Fig. 2 Photographs of the wetting front at increasing times

$$c_s = \left(-0.2274 \times 10^{-\frac{T}{788}} + 0.62\right) \times 1000 \tag{1}$$

$$\lambda_s = -31.1 \times 10^{-\frac{T}{1705}} + 47.7 \tag{2}$$

The jet-cooling system consisted of heating, cooling, and data recording units. The heating equipment consisted of a resistance heating furnace, while the cooling device included mainly a valve, flowmeter, and nozzle. The jet velocity could be adjusted via the flowmeter. Two circular nozzles with a length of 90 mm, inner diameter of 3 mm, and spacing of 60 mm were fixed above the target plate. A 20 (thickness) × 80 (width) × 150 (length) mm³ high-alumina refractory brick was placed under the target plate to maximize the heat insulation for the lower surface. The jet height z and flow Q used in this study are shown in Table 1, while the jet exit velocity u was calculated through the flow. During the experiment, the plate was heated to an average temperature of 938.2 °C in the furnace and then transferred to the refractory brick. At the beginning of the cooling process, an iron box was used to collect water; such box was removed when the water flow was stable. The jet stagnation point was located on the upper surface, above P1-3, and the water curtain caused by the intersection of the two jets was located on the upper surface, above P1-1. The data-recording module was composed of thermocouples, a multi-channel temperature-data collector,

and a computer. The temperature-data collector was used to record the various temperatures at different points by converting the electrical signal into a temperature signal and storing them in the connected computer.

The error of the K-type thermocouple was approximately ± 1.0 %. The jet flow was controlled within ± 3 L/h, and the jet height error was within ± 3 mm. The deviation distance of the thermocouples and jet point was within ± 0.5 and ± 1 mm, respectively. For the different experimental conditions, the initial cooling temperature error did not exceed 0.9 %.

A nine-point moving average method was used to reduce the temperature noise. Assuming that the average noise for all temperature values was zero, the true temperature could be calculated according to:

$$Y_{k,M} = \frac{\sum_{i=1}^n (x_{M-i} + x_{M+i}) + x_M}{2n + 1} \tag{3}$$

where, $Y_{k,M}$ is the filtered temperature at point K and time M , x_{M-i} is the measured temperature at time $M-i$, and n represents the radius of the sliding window, here set to four.

The ability of the fluid-cooling plate was evaluated via the heat flux. Based on the temperature history, the surface heat flux could be calculated through the inverse heat conduction. The solution method used in this work has been provided in a previous study [18]. According to the calculation results, the

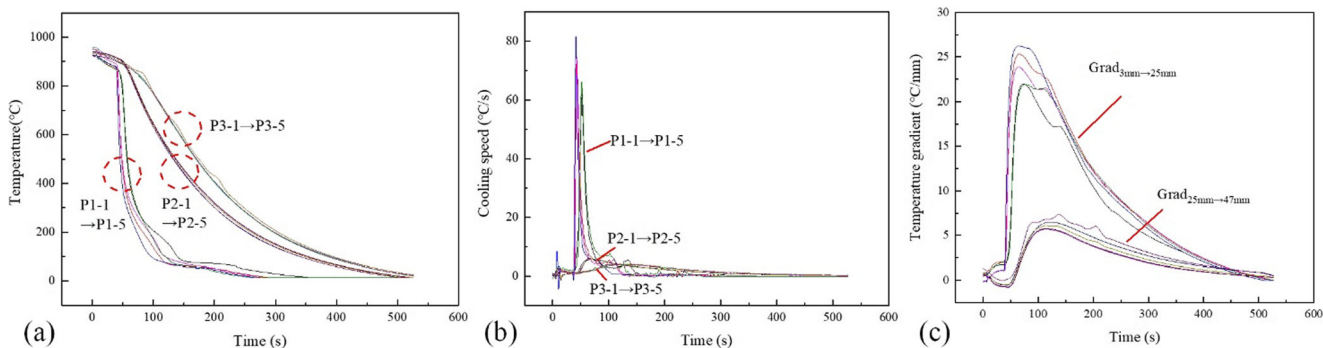


Fig. 3 a Temperature curve, b cooling speed curve, and c temperature gradient curve

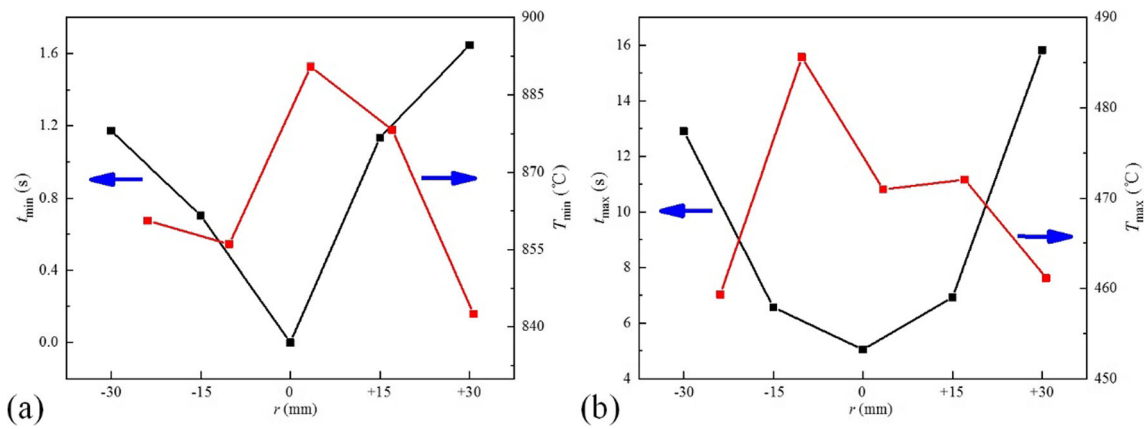


Fig. 4 **a** Rewetting time and temperature; **b** complete-wetting time and temperature

relative error did not exceed 0.1 %, 1.5 %, and 3.7 % at $h = 3$, 25, and 47 mm, respectively, and the largest errors were found to occur at points far away from the coolant surface. Therefore, it was possible to infer that the estimated surface heat flux has a sufficiently high calculation accuracy.

3 Experimental results and discussions

In order to simplify the discussion, several points and terms are here defined. When the boiling structure changed from film boiling to transition boiling, the wall was rewetted [19, 20] (the wall color changed from red to gray, and the heat flux began to increase explosively), and the occurrence time and surface temperature were denoted as the rewetting time t_{\min} and rewetting temperature T_{\min} . When the boiling structure changed from transition boiling to nucleate boiling, the wall was completely wetted (the wall color changed from gray to dark, and the heat flux reached its maximum value q_{\max}), and the occurrence time and surface temperature were denoted as the complete-wetting time t_{\max} and complete-wetting

temperature T_{\max} . The point on the upper surface above P1-1 to P1-5 was marked as P0-1 to P0-5, respectively, and P0-3 was rewetted at $t = 0$ s.

3.1 Double-jet heat transfer characteristics

The heat transfer characteristics for the double-jet experiments were investigated at $z = 150$ mm and $u = 2.95$ m/s. Figure 2 shows that the wetting front can be clearly distinguished and that the rewetting and complete-wetting occur on its outer and inner edges, respectively. As times passes, a varying wetting front width can be observed. When $t = 0.72$ s, the wetting front width rapidly increases to approximately 17.5 mm; according to Fig. 2, this phenomenon appears to be related to the deflection fluid of the jet along the wall. Afterwards, the width decreases to 1.82 mm at $t = 0.90$ s. Woodfield et al. [9] reported that such decrease is caused by the increased radial temperature gradient. At $t = 1.19$ s, the width increases again to 5.4 mm. This might be due to the decreased flow velocity, which reduces the ability for the fluid to sweep bubbles at the wetting front, thus resulting in an increasing width.

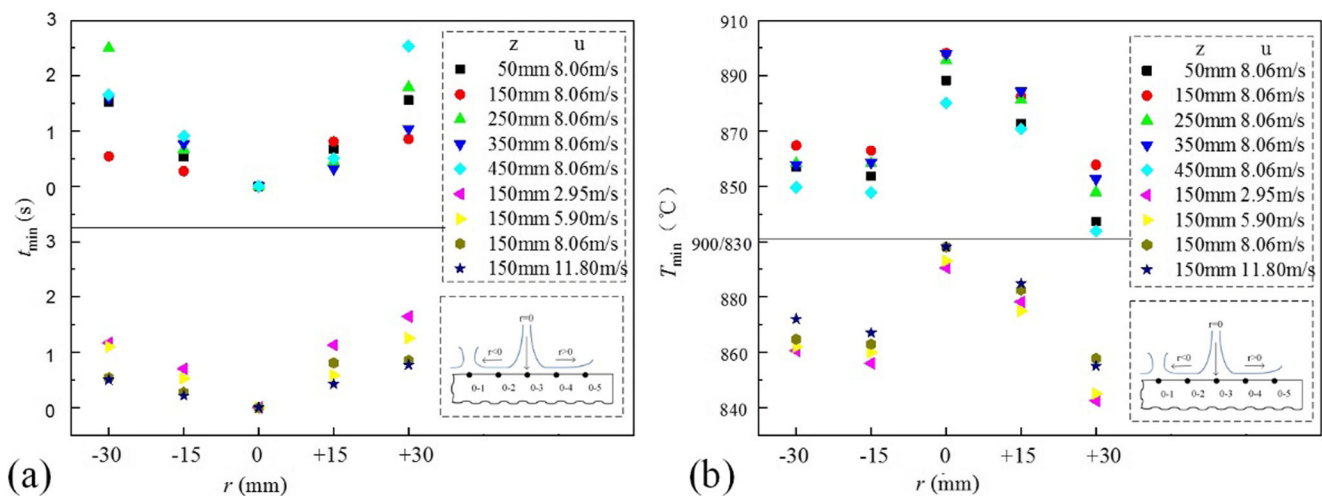


Fig. 5 Characteristic values for the rewetting phenomenon at $z = 50$ –450 mm and $u = 2.95$ –11.80 m/s: **a** rewetting time and **b** rewetting temperature

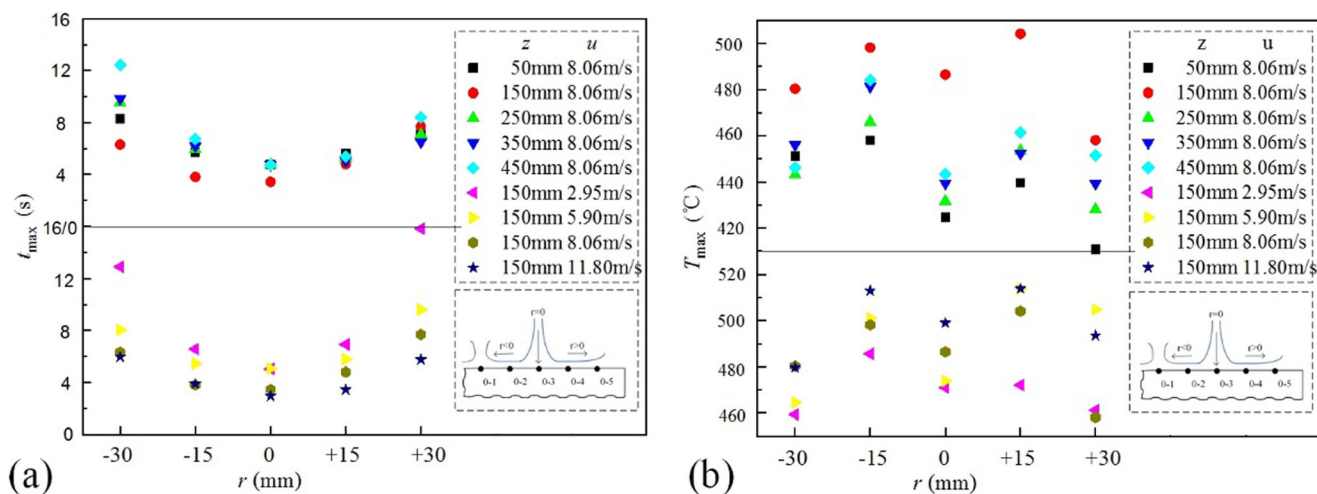


Fig. 6 Characteristic values for the complete-wetting phenomenon at $z = 50\text{--}450$ mm and $u = 2.95\text{--}11.80$ m/s: **a** time and **b** temperature

The measured temperature curves are shown in Fig. 3a. The slow cooling stage before jet cooling is attributed to the transfer of the target plate. Upon starting the experiment, it can be seen that the temperature at P1-1 to P1-5 rapidly decreases to below 200 °C within 48.4 s on average, and the average temperature at $h = 25$ and 47 mm is 705.3 and 817.9 °C, respectively. The temperature increases with the increased distance between the point and cooled surface until the end of the cooling process. The cooling speed (temperature gradient with respect to time) and temperature gradient as a function of time are shown in Fig. 3b-c. For $h = 3$ mm, the cooling speed and temperature gradient begin to increase rapidly at 38.4 s (approximately the time at which the plate is transferred), while for $h = 25$ mm a significant increase occurs at 43.3 s, which explains the hysteresis of the cooling process away from the surface. $Grad_{3mm \rightarrow 25mm}$

(temperature gradient between $h = 3$ mm and $h = 25$ mm) keeps growing until the cooling speed at $h = 3$ mm becomes equal to that at $h = 25$ mm, and $Grad_{25mm \rightarrow 47mm}$ was found to have a similar change to $Grad_{3mm \rightarrow 25mm}$. The average maximum cooling speed at $h = 3, 25,$ and 47 mm was measured to be 71.87, 5.86, and 4.07 °C/s, respectively. The above results prove that the temperature gradient determines the cooling speed field.

Figure 4a shows the t_{min} and T_{min} at $z = 150$ mm and $u = 2.95$ m/s. Due to the frictional resistance and vapor film, it takes a certain amount of time for the fluid to rewet the surface, and t_{min} increases along both sides from P0-3. Most researchers have found that, within a certain range of jet diameters, the fluid is deflected away from the surface due to the deflection force caused by bubbles at the wetting front [19–21]. In this study,

Fig. 7 Maximum heat flux at $z = 50\text{--}450$ mm and $u = 2.95\text{--}11.80$ m/s

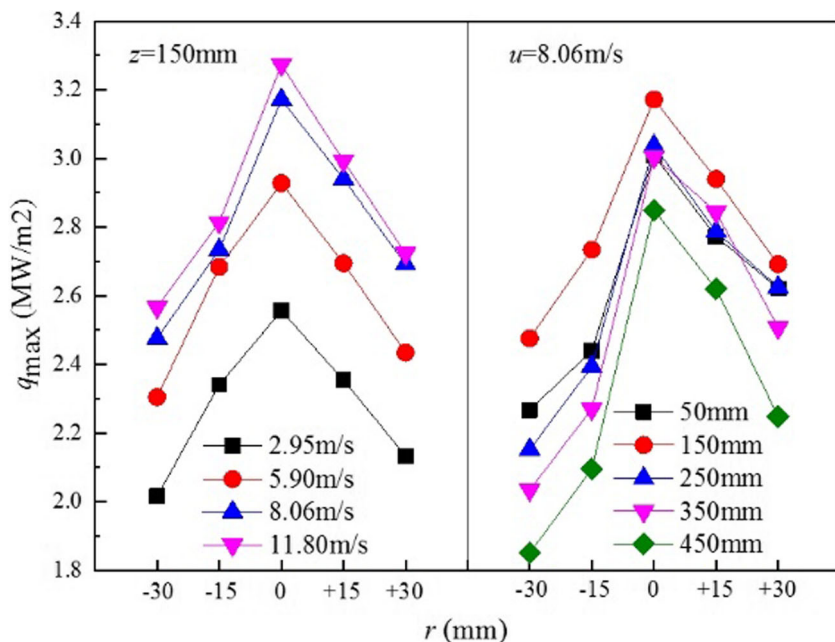
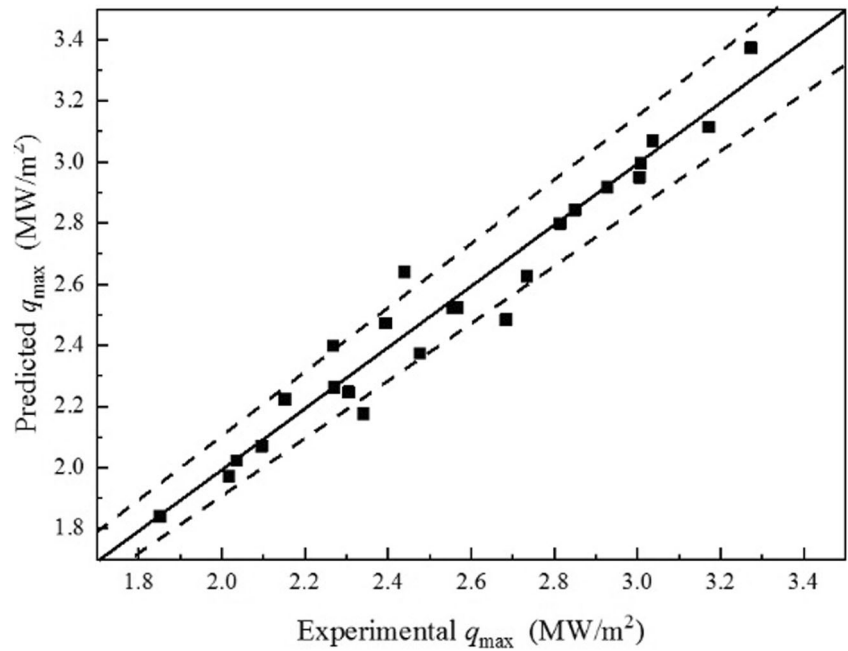


Fig. 8 Comparison between the predicted and experimental values of q_{\max}



the deflected fluid can be observed in Fig. 2, but the deflection has no effect on the rewetting phenomenon due to the splashing out of the test area. As momentum decreases and fluid temperature increases, it can be seen that T_{\min} decreases with increasing the radial distance (for $r = -15, +15,$ and $+30$ mm). At $r = -30$ mm, T_{\min} is slightly higher than at $r = -15$ mm, since the accumulated water curtain increases the fluid supply before rewetting. In addition, the fluid layer in the confluence jet region prolongs the film boiling duration, and a lower T_{\min} is thus observed compared with that in the wall jet region.

t_{\max} and T_{\max} are shown in Fig. 4b. P0-3 is impacted by the jet and completely wetted first. t_{\max} is the lowest at P0-3 and gradually increases along both sides. It should be noted that a local minimum for T_{\max} is observed at P0-3. This might be due to the high-pressure fluid at the jet region reducing the bubble circulation frequency and enhancing heat convection

in the transition boiling, resulting in a lower surface temperature. At $r = \pm 15$ mm, T_{\max} was found to be higher than at $r = 0$, due to the increased bubble circulation frequency, with an average increase of 7.86 °C. Afterwards, the decreased flow velocity and increased fluid temperature lead to a low heat transfer, with the minimum T_{\max} occurring at $r = \pm 30$ mm.

3.2 Influence of the jet parameters on the rewetting and complete-wetting phenomena

The rewetting time and rewetting temperature for different values of u and z are shown Fig. 5. As u increases from 2.95 to 11.80 m/s, the impinging stream accumulates into a higher turbulence zone, which results in an accelerations of the rewetting speed. t_{\min} was found to be reduced by 0.67 and

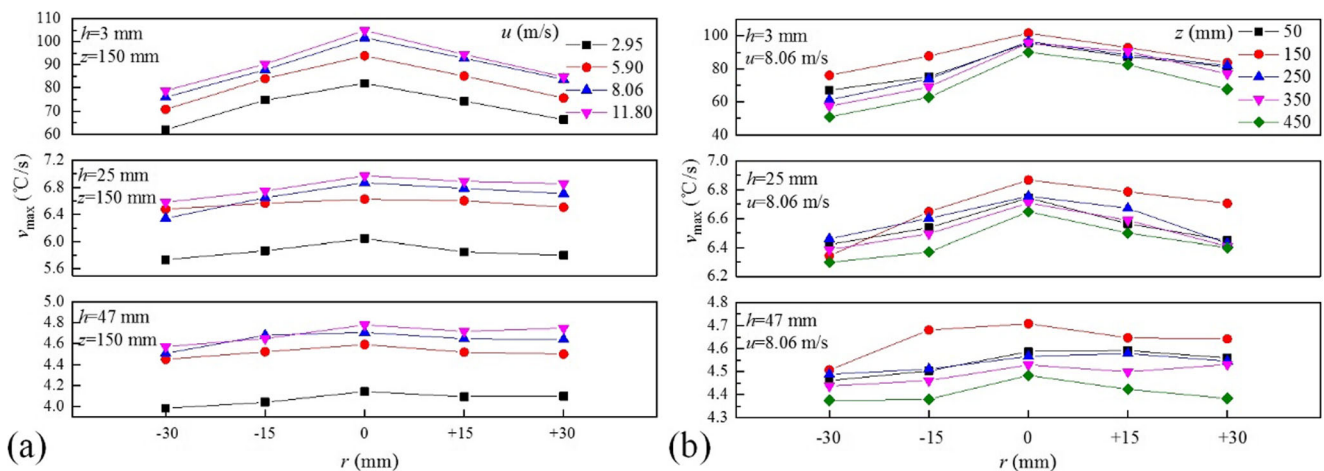


Fig. 9 Maximum cooling speed at $h = 3, 25, 47$ mm: **a** $z = 150$ mm and $u = 2.95\text{--}11.80$ m/s and **b** $z = 50\text{--}450$ mm and $u = 8.06$ m/s

Table 2 Parameters used in the power-law relationship

	a'	b'	c'	d'	e'
A_0	3.591	0.111	0.980	2.496×10^{-4}	-7.063×10^{-7}
A_1	91.426	0.186	0.913	9.108×10^{-4}	-2.802×10^{-6}

0.88 s at $r = -30$ and $+30$ mm, respectively, while T_{\min} was observed to increase by 9.85 °C on average. According to Fig. 5a, it can be inferred that u has a lower influence on the confluence jet region, and a possible reason for this phenomenon might be that the accumulated fluid layer weakens the u influence. When changing z , the interference and interaction between the two jets are also changed. However, the same variation of the rewetting parameter as a function of z can be observed for the wall jet region and confluence jet region, as shown in Fig. 5b. With the increase of z , t_{\min} firstly decreased and then increased, T_{\min} followed the opposite trend. The lower fluid splash volume and faster fluid velocity lead to a smaller t_{\min} and higher T_{\min} at $z = 150$ mm.

The complete-wetting time and complete-wetting temperature for different values of u and z are shown Fig. 6. As u increases, the high-momentum fluid accelerates the bubble detachment rate from the surface and prevents bubbles from accumulating in the wetting front [17], which promotes the structure changing from transition boiling to nucleate boiling. A decreased t_{\max} and increased T_{\max} are observed. As the converging fluid provides a stronger turbulence while reducing the fluid momentum, no significant difference for t_{\max} and T_{\max} can be observed between the confluence jet region and wall jet region. For $z = 150$ mm, the high kinetic energy of the fluid, which is caused by the lower fluid splash volume and faster fluid velocity, enhances the ability of the fluid to sweep the bubbles, leading to the lowest t_{\max} and highest T_{\max} . According to Fig. 6a, the impact of z on the confluence jet region is particularly evident. The changing rate of t_{\max} increases radially from $r = 0$ mm to $r = -30$ mm, with values of 10.15 and 25.24 % at P0-3 and P0-1, respectively. This indicates that, in the confluence jet region, as the distance from the jet point increases, the offset of the fluid momentum caused by the opposite motion of the jets reduces the ability to sweep the bubbles at the wetting front, and the transition boiling duration is thus extended. By calculating the difference between T_{\min} and T_{\max} , the temperature drop at P0-1 was found to be lower than that at P0-5 from t_{\min} to t_{\max} . Therefore, it can be inferred

that an excessive amount of the accumulated fluid reduces the heat transfer efficiency in the transition boiling.

3.3 Maximum heat flux and correlation

Figure 7 shows q_{\max} in different regions at $u = 2.95$ – 11.80 m/s and $z = 50$ – 450 mm. Due to the friction resistance and enthalpy increase, the heat transfer ability between the fluid and wall is slowed down, and q_{\max} in the confluence jet region and wall jet region was found to be lower than in the jet region. In the wall jet region, a larger q_{\max} value was obtained at a high T_{\min} , which proves that the rewetting temperature affects the maximum heat flux. The radial range from P0-3 to P0-2 also follows this rule. T_{\min} at P0-1 was found to be higher than at P0-2, but a lower q_{\max} was obtained, which might be related to the lower T_{\max} caused by the confluence fluid. A lower T_{\max} reduces the bubble boiling circulation frequency and heat convection intensity, thus leading to a low q_{\max} . Therefore, based on the above discussion, it can be concluded that q_{\max} is affected by both T_{\min} and T_{\max} , the former being the dominant factor.

The actual cooling process was more similar to that in the jet region and confluence jet region. According to the experimental data, a correlation of the maximum heat flux at the jet point $(q_{\max})_0$ was established, and the equation was extended to other locations in the confluence jet region $(q_{\max})_r$:

$$(q_{\max})_0 = u^{0.21} \times 2.03 \times (9.00 \times 10^{-1} + 1.17 \times 10^{-3}z - 4.71 \times 10^{-6}z^2 + 4.68 \times 10^{-9}z^3) \quad (4)$$

$$(q_{\max})_r / (q_{\max})_0 = 3.84 \times 10^2 - 2.55z - 4.75 \times 10u + 3.2 \times 10^{-1}zu - 5.42 \times 10^{-3}r \quad (5)$$

where r is the distance from the jet point ($0 \leq r \leq 30$) in mm, u is the jet exit velocity ($2.95 \leq u \leq 11.80$) in m/s, and z is the jet height ($50 \leq z \leq 450$) in mm.

q_{\max} was found to be directly proportional to $u^{0.21}$, rather than to $u^{1/3}$, as was reported by most previous works [22–24].

Table 3 Prediction errors

u (m/s)	2.95	5.90	8.06	11.80	8.06	8.06	8.06	8.06
z (mm)	150	150	150	150	50	250	350	450
$h = 3$ mm	0.53 %	0.97 %	2.92	-1.47 %	-1.93	-4.55 %	0.37 %	6.02 %
$h = 25$ mm	-0.51	-1.35 %	-1.14	-4.36 %	-1.17	-1.53 %	1.29 %	6.99 %
$h = 47$ mm	-0.86 %	1.67 %	0.81	-2.29 %	-0.17	-1.00	-0.18 %	1.38 %

The reason might be that the temperature change caused by the jet impingement is weakened in thick plates due to the plate heat conduction. Agrawal et al. [15] and Paul et al. [16] respectively proposed that q_{\max} is directly proportional to $(z/d)^{-0.01}$ and $(z/d)^{0.086}$, with $z/d=4-16$ and $z/d=4-10$. However, considering the flatness and deformation of the plate, the above z/d relationship was not applicable for the thick plate. In this study, the jet height range was $16 < z/d \leq 150$, and q_{\max} was found to increase first and then decrease with the increase of z , which is not in agreement with a trend of the form $(z/d)^n$. Therefore, a one-dimensional cubic equation was used. The proposed correlation could well predict the q_{\max} value from P0-3 to P0-1. The maximum error band in Fig. 8 is $\pm 5\%$, and the predicted value falls within the error band within 85% probability.

3.4 Maximum cooling speed and correlation

The maximum cooling speed v_{\max} at different measurement points is shown in Fig. 9. The internal cooling speed is mainly affected by the heat conduction along the thickness and exhibits the same variation trend as the surface heat flux: it increases with the increase of u , and it firstly increases and then decreases with the increase of z . For $z=150$ mm and $u=8.06$ m/s, the v_{\max} difference along the horizontal direction at $h=3$ mm was found to be 24.55%, while it reduces to 4.26% at $h=47$ mm. The data prove that the horizontal heat conduction plays an important role in the v_{\max} movement process along the thickness. One of the aims of this study was to explore the cooling-speed field along the thickness. Therefore, according to the above results, the average maximum cooling speed along the horizontal v_{ave} was used to establish correlations with u , z , and h .

The varying trend of v_{ave} along h can be predicted using the function model $V_{\text{ave}} = A_0 + A_1 \times e^{(-h/A_2)}$, in which A_0 , A_1 , and A_2 are related to u and z . The power-law relationship of A_0 and A_1 with u and z is: $A = a' \times u^{b'} \times (c' + d' \times z + e' \times z^2)$, where the a' , b' , c' , d' , and e' values are shown in Table 2, and A_2 is here assumed to be 6.1. The proposed correlation could be used to predict 93% of the experimental results within $\pm 5\%$ error as shown in Table 3.

4 Conclusions

To understand the heat-transfer characteristics and cooling-speed field for a thick plate with multiple jets, double water-jet cooling experiments were performed on a 50 mm thick plate at jet exit velocities of 2.95–11.80 m/s and jet heights of 50–450 mm. The main results are as follows:

- (1) The wetting front width is affected by the radial temperature gradient and fluid motion and appears to have a complex trend, with sequential increasing, decreasing, and increasing behaviors upon increasing the wetting region diameter.
- (2) The accumulated water curtain can increase the fluid supply before rewetting, thus raising the rewetting temperature. However, its effect on the complete-wetting phenomenon was not observed. It is speculated that an excessive amount of the accumulated fluid would reduce the heat transfer efficiency in the transition boiling.
- (3) The confluence fluid layer between the two jets reduces the influence of different jet velocities, but enhances the complete-wetting parameters difference in the confluence jet region for different jet heights due to the prolonged transition boiling duration.
- (4) The heat flux can be adjusted via the rewetting temperature and complete-wetting temperature, and the cooling speed field variation along the thickness was provided.

Nomenclature ρ_s , density of the experimental material Kg/m^3 ; c_s , specific heat of the experimental material $\text{J}/(\text{kg}\cdot\text{K})$; h , the distance to the cooled surface mm; t , cooled time s; z , jet height mm; Q , jet flow L/h ; u , jet exit velocity m/s; Y , filtered temperature $^\circ\text{C}$; x , measured temperature $^\circ\text{C}$; K , measured point mm; M , time step s; λ_s , thermal conductivity of the experimental material $\text{W}\cdot(\text{m}\cdot\text{K})^{-1}$; r , the horizontal distance between the surface position and jet point; mm; t_{\min} , rewetting time s; T_{\min} , rewetting temperature $^\circ\text{C}$; t_{\max} , complete-wetting time s; T_{\max} , complete-wetting temperature $^\circ\text{C}$; q_{\max} , the maximum heat flux MW/m^2 ; d , nozzle diameter mm; Grad, temperature gradient $^\circ\text{C}/\text{mm}$; v_{\max} , the maximum cooling speed $^\circ\text{C}/\text{s}$; v_{ave} , the average maximum cooling speed along the horizontal $^\circ\text{C}/\text{s}$

Funding This work was supported by the National Key Research and Development Programs of China (Grant number [2017YFB0305102]).

Declarations

Conflict of interest The authors have no conflicts of interest to declare that are relevant to the content of this article.

References

1. Seraj MM, Mahdi E, Gadala MS (2012) Numerical assessments of impingement flow over flat surface due to single and twin circular long water jets. *Trans Control Mech Trans Control Mech Syst* 1: 290–299
2. Sharma AK, Modak M, Sahu SK (2018) The heat transfer characteristics and rewetting behavior of hot horizontal downward facing surface by round water jet impingement. *Appl Therm Eng* 138: 603–617
3. Agrawal C, Kumar R, Gupta A, Chatterjee B (2012) Effect of jet diameter on the rewetting of hot horizontal surfaces during quenching. *Exp Therm Fluid Sci* 42:25–37

4. Nobari AH, Prodanovic V, Militzer M (2016) Heat transfer of a stationary steel plate during water jet impingement cooling. *Int J Heat Mass Trans* 101:1138–1150
5. Mozumder AK, Monde M, Woodfield PL, Islam MA (2006) Maximum heat flux in relation to quenching of a high temperature surface with liquid jet impingement. *Int J Heat Mass Trans* 49: 2877–2888
6. Agrawal C, Kumar R, Gupta A, Chatterjee B (2013) Effect of jet diameter on the maximum surface heat flux during quenching of hot surface. *Nucl Eng Des* 265:727–736
7. Qiu L, Dubey S, Choo FH, Duan F (2015) Recent developments of jet impingement nucleate boiling. *Int J Heat Mass Trans* 89:42–58
8. Mozumder AK, Monde M, Woodfield PL (2005) Delay of wetting propagation during jet impingement quenching for a high temperature surface. *Int J Heat Mass Trans* 48:5395–5407
9. Woodfield PL, Mozumder AK, Monde M (2009) On the size of the boiling region in jet impingement quenching. *Int J Heat Mass Trans* 52:460–465
10. Karwa N, Gambaryan Roisman T, Stephan P, Tropea C (2011) Experimental investigation of circular free-surface jet impingement quenching: Transient hydrodynamics and heat transfer. *Exp Therm Fluid Sci* 35:1435–1443
11. Hatta N, Kokado JI, Hanasaki K (1983) Numerical analysis of cooling characteristics for water bar. *Trans ISIJ* 23:555–564
12. Mozumder AK, Woodfield PL, Islam MA, Monde M (2007) Maximum heat flux propagation velocity during quenching by water jet impingement. *Int J Heat Mass Trans* 50:1559–1568
13. Ravikumar SV, Jha JM, Mohapatra SS, Pal SK, Chakraborty S (2014) Experimental investigation of effect of different types of surfactants and jet height on cooling of a hot steel plate. *J Heat Trans* 136:072102-1-072102–10
14. Barewar SD, Tawri S, Chougule SS (2019) Heat transfer characteristics of free nanofluid impinging jet on flat surface with different jet to plate distance. *Chem Eng Process* 136:1–10
15. Agrawal C, Kumar R, Gupta A, Chatterjee B (2012) Rewetting and maximum surface heat flux during quenching of hot surface by round water jet impingement. *Int J Heat Mass Trans* 55:4772–4780
16. Paul G, Das PK, Manna I (2015) Rewetting of vertical pipes by bottom flooding using nanofluid as a coolant. *J Heat Trans* 137: 121009–121001
17. Wang B, Lin D, Xie Q, Wang Z, Wang G (2016) Heat transfer characteristics during jet impingement on a high-temperature plate surface. *Appl Therm Eng* 100:902–910
18. Tian XH, Fu TL, Zhang JW, Wang ZD, Wang GD (2020) Effect of nanofluids on liquid-solid heat transfer on high-temperature wall. *ISIJ Int* 60:1993–1999
19. Hall DE, Incropera FP, Viskanta R (2001) Jet impingement boiling from a circular free-surface jet during quenching: part 2—two-phase jet. *J Heat Trans* 123:911–917
20. Hall DE, Incropera FP, Viskanta R (2001) Jet impingement boiling from a circular free-surface jet during quenching: Part 1—single phase jet. *J Heat Trans* 123:901–909
21. Karwa N, Stephan P (2013) Experimental investigation of free-surface jet impingement quenching process. *Int J Heat Mass Trans* 64:1118–1126
22. Qiu Y, Liu Z (2005) Critical heat flux in saturated and subcooled boiling for R-113 jet impingement on the stagnation zone. *Appl Therm Eng* 25:2367–2378
23. Liu Z, Zhu Q (2002) Prediction of critical heat flux for convective boiling of saturated water jet impinging on the stagnation zone. *J Heat Trans* 124:1125–1130
24. Liu Z, Tong T, Qiu Y (2004) Critical heat flux of steady boiling for subcooled water jet impingement on the flat stagnation zone. *J Heat Trans* 126:179–183

Publisher's note Springer Nature remains neutral with regard to jurisdictional claims in published maps and institutional affiliations.